ELSEVIER

International Journal of Heat and Fluid Flow 21 (2000) 589–598

International Journal of HEAT AND FLUID FLOW

www.elsevier.com/locate/ijhff

Numerical simulation of the interactions of highly entangled polymers with coherent structure in a turbulent channel flow

Y. Hagiwara [a,*], H. Hana [b], M. Tanaka [a], S. Murai [c]

[a] *Department of Mechanical and System Engineering, Kyoto Institute of Technology, Goshokaido-cho, Matsugasaki, Sakyo-ku, Kyoto 606-8585, Japan*
[b] *Kubota Co. Ltd, Osaka, Japan*
[c] *Graduate School of Mechanical and System Engineering, Kyoto Institute of Technology, Kyoto, Japan*

Abstract

Direct numerical simulations have been conducted with many cluster models of beads and connecting springs in a turbulent channel flow in order to investigate how the low-speed streaks and the small-scale flow related to the streaks are affected by the cluster models. The cluster model represents highly entangled polymers observed in the quiescent and flowing aqueous solution. The cluster models were introduced in the buffer region to simulate the experiments of Tiederman et al. (Tiederman, W.G., Luchik, T.S., Bogard, D.G., 1985. Wall-layer structure and drag reduction. J. Fluid Mech. 156, 419–437) in which the polymer solution was injected from a slot in the channel wall. An experiment has been carried out for visual observation of highly entangled polymers in a turbulent channel flow of the same Reynolds number in order to determine a parameter of the cluster model. The computational results show that the minor streaks and the small-scale eruptive flows associated with the streamwise vortices are attenuated selectively by the cluster models. The length scale and time scale of these structures are comparable to those of the cluster model. On the other hand, the dynamics of large-scale streaks are found to be basically unchanged. These results are consistent with the measurement of a suppression of low threshold Reynolds-stress producing motion by Harder and Tiederman (Harder, K.J., Tiederman, W.G., 1991. Drag reduction and turbulent structure in two-dimensional channel flows. Philos. Trans. R. Soc. Lond. 336, 19–34). © 2000 Begell House Inc. Published by Elsevier Science Inc. All rights reserved.

Keywords: Turbulent drag reduction; Dilute polymer solution; Cluster model of beads and springs; DNS; Minor streaks; Eruptive flow

1. Introduction

Near-wall coherent structures in turbulent channel flows of dilute polymer solutions have been focused on in order to understand the mechanism of drag reduction by polymers. Oldaker and Tiederman (1977) measured an increase in the spacing of low-speed streaks caused by polyethylene oxide (PEO) or polyacrylamide (PAM). Tiederman et al. (1985) reported a decrease in the bursting rate and an increase in the streak spacing for a water channel flow with an injection of dilute PAM solutions from a slot into a buffer region. Harder and Tiederman (1991) confirmed experimentally that small-amplitude Q2 and Q4 events are damped in drag-reduced flow with the injection of polymers into the buffer region while the large amplitude events are unaffected. Similarly, a suppression of ejection and sweep was concluded by Gampert and Yong (1990) from their measurement of Q2 and Q4 events in a turbulent channel flow for uniform solution of PAM.

The effect of the polymers on the coherent structure has been examined numerically recently in more detail. Direct numerical simulation (DNS) was used for the solvent flow. Orlandi (1995) and den Toonder et al. (1997) introduced an anisotropic model for the viscosity to express the polymer effects on solvent flows, and predicted the modification of coherent structures due to the polymers. Sureshkumar et al. (1997) reproduced the decrease in the bursting rate by modifying the stress tensors based on the finitely-extendable-nonlinear-elastic (FENE) model for their DNS. This model consists of two spherical beads and a connecting spring with a nonlinear spring constant, and is representative of polymer chains. Massah and Hanratty (1997) predicted an additional dissipation of energy by use of several FENE models in their DNS. Kajishima and Miyake (1998) reproduced the reduction of Reynolds shear stress and an increase in streak spacing using many beads–spring–dashpot models in their DNS.

However, it was hardly possible that the entangled polymers were simulated by the models. These polymers were observed for a long period in the solution, which is produced by gentle mixing of polymer powders with water to avoid mechanical degradation of the polymers (Hagiwara et al., 1998). The aggregated polymers can exist in a turbulent

* Corresponding author. Tel.: +81-75-724-7324; fax: +81-75-724-7300.
E-mail address: yoshi@ipc.kit.ac.jp (Y. Hagiwara).

0142-727X/00/$ - see front matter © 2000 Begell House Inc. Published by Elsevier Science Inc. All rights reserved.
PII: S0142-727X(00)00049-7

Notation

D	equivalent diameter of cluster
$\boldsymbol{F}_D$	drag force
$\boldsymbol{F}'_D$	reaction to drag force
$\boldsymbol{F}_S$	restitution force
h	half height of duct
k	spring constant
L_R	streamwise dimension of contours
L_T	distance for the cluster model to be transported
L_1, L_3	dimensions of computational domain in the X_1 and X_3 directions
l_{mn}	length of spring connecting mth bead and nth bead
l_{mn0}	initial value of l_{mn}
l_c	critical length for spring
N_1, N_2, N_3	numbers of grid points in the X_1, X_2 and X_3 directions
P	pressure
Re^*	Reynolds number based on u^* and h
r	bead radius
t	time
$\boldsymbol{U}$	carrier fluid velocity
$\boldsymbol{U}^m$	velocity of mth bead
U_1, U_2, U_3	instantaneous velocities in the X_1, X_2 and X_3 directions
$\overline{U}_1$	streamwise mean velocity
u_1, u_2, u_3	fluctuating velocities in the X_1, X_2 and X_3 directions
u^*	friction velocity
V	cell volume
$\boldsymbol{X}^m$	location of mth bead
X_1, X_2, X_3	coordinates in the streamwise, wall-normal and transverse directions
Greeks	
ΔX_1, ΔX_2, ΔX_3	grid spacing in the X_1, X_2 and X_3 directions
λ	relaxation time for dumbbell model
μ	viscosity
ν	kinematic viscosity
ρ	density
τ	relaxation time for solid body
ω_1	streamwise vorticity

channel flow with injection of the polymer solution (Hagiwara et al., 1998) and the channel flows for uniform polymer solution (Willmarth et al., 1987; Warholic et al., 1999). The dimension of the entangled polymers is larger than the smallest length scale of turbulence. We developed a cluster model of beads and springs as representative of highly entangled polymers (Hagiwara et al., 1997). Our model was based on irregular network structures in bundles of polymers, which were observed in the freeze-dried samples from the flows of dilute PEO solutions by James and Saringer (1980) and Miyamoto (1994). We carried out DNS on turbulent channel flow with several cluster models in the buffer region and showed the small-scale eddy was influenced by the models (Hagiwara et al., 1997).

In the present study, DNS is carried out for turbulent channel flow with many cluster models in the buffer region in order to simulate the experiment conducted by Tiederman et al. (1985). Visual observation is also done for estimating a parameter of the model. Not only the turbulence quantities but also direct interaction between the cluster models and the low-speed streaks or the streamwise vortices near the streaks are examined in order to understand the attenuation of the Q2 event. Comparison of the Reynolds-stress product at a typical moment in the case with the cluster models with that in the case without the models is tried to examine this interaction. Direct interaction between the cluster models and the small-scale eruptive flow in the large-scale streak is also investigated.

2. Cluster model of beads and springs

2.1. Assumptions

Fig. 1(a) shows the sketch from a photograph from Miyamoto (1994). Strands which consist of a bundle of polymer chains and nodes where the strands are entangled are recognised in the irregular network structure in the photograph. We assumed that the nodes were replaced by spherical beads whose density is the same as that of the solvent flow. This is reasonable because the nodes take a long time for their dissolution and the nodes can be considered to be impermeable for a certain period of the dissolution. It was also assumed that the beads are of identical size, for simplicity.

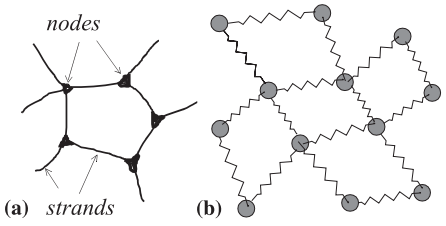

Fig. 1. Observed polymers and cluster model.

Next, we assumed that the strands were replaced by nonlinear springs with no volume. The restitution force of springs was similar to that of an FENE model, and the spring constant was identical. If the distance between any two beads was longer than the critical length, l_c, these beads were assumed not to be connected directly by a spring. l_c was 1.99 times larger than the initial length of each spring. If a spring is longer than two times of its initial value, it gives an unrealistic restitution force from the definition of the force in the equation mentioned below. New entanglement of polymers or the formation of the network structure can be achieved by adding springs between the beads, while the breakup of the structure can be achieved by subtracting the springs. Fig. 1(b) illustrates part of the cluster.

Finally, the connection between any two beads of two different cluster models was not considered for simplicity. This is reasonable when the polymer concentration is low and not completely uniform.

2.2. Motion of beads

The drag force, $\boldsymbol{F}_D$, calculated by the Stokes law of resistance and the restitution force of the spring, $\boldsymbol{F}_S$, were considered to act on the beads. The equation of motion for the mth bead is as follows:

$$\rho\frac{4\pi r^3}{3}\frac{\partial \boldsymbol{U}^m}{\partial t} = -\boldsymbol{F}_{\mathrm{D}}^m + \boldsymbol{F}_{\mathrm{S}}^m = -6\pi\mu r(\boldsymbol{U}^m - \boldsymbol{U}) + \sum_{n=1}^{N}\frac{k}{1-(l_{mn}-l_{mn0})^2/l_{mn0}^2}\frac{l_{mn0}-l_{mn}}{l_{mn}}(\boldsymbol{X}^m - \boldsymbol{X}^n), \tag{1}$$

where ρ is the bead density, r the bead radius, $\boldsymbol{U}^m$ and $\boldsymbol{U}$ the velocities of the bead and the solvent flow at the bead's location respectively, μ the solvent viscosity, N the total number of springs connected to the mth bead, l_{mn} and l_{mn0} the distance between the bead and the nth bead and its unloaded value, respectively, $\boldsymbol{X}^m$ and $\boldsymbol{X}^n$ the positions of the mth and nth beads, respectively, and k is the spring constant.

$\boldsymbol{U}^m$ was evaluated by the time integration of a discrete form of Eq. (1). The second-order Adams–Moulton method was used for the time integration. Note that the Reynolds number based on the bead diameter and the velocity difference between the bead and the ambient fluid was lower than 1.5, and hence the Stokes law was satisfied. The location of the bead was calculated by the second-order Adams–Moulton method (Pan and Banerjee, 1996).

2.3. Length scales and spring constant

Table 1 compares the dimensions for the highly entangled polymers estimated from the results by Miyamato and our observation mentioned below with those for the cluster model in the present study. These values are in the nondimensional forms by using the friction velocity, u^*, of the present DNS, the kinematic viscosity, ν, and the channel height in our experiment. The values with brackets in the table indicate the initial values. The underlined value in the table denotes the experimental result obtained by the present authors. The cluster volume in the table is calculated from the initial region of either $29.4\nu/u^* \times 14.7\nu/u^* \times 14.7\nu/u^*$ (rectangular prisms) or $14.7\nu/u^* \times 14.7\nu/u^* \times 14.7\nu/u^*$ (cube) for each cluster model. We estimated the apparent spring constant from Miyamoto's discussion in which he calculated the stress, and the ratio of the length in the shear direction for a mesh in the network structure and that perpendicular to the direction. It is found from this table that all the values for the cluster model are realistic and reasonable.

We assumed that 64 beads were allocated regularly in each cluster model at the initial state in the case where the region for each model was the cube, and 128 beads in the case where the region was the rectangular prism. The unloaded spring length, l_{mn0}, was assumed to be equal to the initial distance between two neighbouring beads.

Table 1
Parameters of the cluster model

	Miyamoto	Cluster model
Shear rate	0.28	0.2–1.0 (buffer region)
Concentration (ppm)	500	450 (buffer region)
Volume	$\underline{1.5\text{–}12\times10^3}$	$[3.2\times10^3]$
Node (bead)		
Diameter	0.24–0.56	1.0
Number density	0.032	[0.020]
Strand		
Thickness	0.075–0.15	0
Length	1.05–3.0	[4.9]
Critical length	–	9.8
Spring constant	0.27	0.2

2.4. Relaxation time

We examined the relaxation time for the FENE model (Massah et al., 1993), λ, and that for an equivalent sphere, τ, as reference time scales for the cluster model. These relaxation times are defined by the following equation:

$$\lambda = \frac{6\pi\mu r}{k}, \quad \tau = \frac{(1/6)\rho\pi D^3}{3\pi\mu D} = \frac{\rho D^2}{18\mu}, \tag{2}$$

where D is the equivalent diameter of the cluster. λ can be considered as the relaxation time for a pair of beads connecting by a spring in the cluster model. τ can be regarded as the relaxation time for the cluster behaving as a solid body due to the tight connection of the beads. λ was equal to $0.31\nu/u^{*2}$, and τ was $1.3\nu/u^{*2}$. The actual characteristic time for the cluster is expected to be in between these relaxation times for two extreme cases.

3. DNS for solvent flow

3.1. Momentum equation

The interaction between the bead of the cluster models and the flow was dealt with as a two-way coupling. The reaction force to the drag force in Eq.(1) was considered to act on the solvent flow as an external point force. The momentum equation of the flow is given as follows:

$$\frac{D\boldsymbol{U}}{Dt} = -\nabla\frac{P}{\rho} + \frac{\mu}{\rho}\nabla^2\boldsymbol{U} + \frac{1}{\rho V}\sum_{m=1}\boldsymbol{F}_{\mathrm{D}}^m, \tag{3}$$

where P is the pressure and V is a cell volume for the reaction force. All the fluid properties were assumed to be equal to that of a Newtonian fluid and constant.

3.2. Computational domain

The computational domain was assumed to be a box of $2\pi h \times 2h \times \pi h$ for a flow between two walls at the distance of $2h$. The origin of the coordinates was at the corner of the lower wall. The X_1, X_2 and X_3 axes were positioned in the streamwise, wall-normal and transverse directions, respectively. The domain was divided into a total of $64 \times 96 \times 64$ cells. The cell dimension is identical either in the X_1 or the X_3 direction. It increases from the walls to the axis based on a hyperbolic tangent. The velocity components were assigned at the centre of the cell surfaces (grid points for velocities), and the pressure and the external force were assigned at the centre of the cell (grid points for forces). The Reynolds number based on h and u^* was 150. The Reynolds number defined by the mean centerline velocity and the wall distance was 5306. In Table 2, the domain size, the number of grid points, the grid spacing, and the Reynolds number are compared with those adopted in DNSs for channel flows with the polymer models (Massah and Hanratty, 1997; Kajishima and Miyake, 1998) and those without the models (Kawamura, 1995; Kuroda et al., 1995).

3.3. Computational schemes

The second-order central difference scheme based on the interpolation method (Kawamura, 1995; Kajishima, 1994; see Appendix A) and that without the method were applied to the finite differencing of the convection terms and the viscous terms of the momentum equations, respectively. The

Table 2
Domain size and grid resolution

Case	L_1/h	L_3/h	N_1	N_2	N_3	ΔX_1^+	ΔX_2^+	ΔX_3^+	Re^*
Present	2π	π	64	97	64	14.7	0.85–5.4	7.36	150
Kajishima	7.7	3.8	64	64	64	18	0.93–9.0	9.0	150
Massah (without polymer model)	13	6.3	128	65	128	14.8	NA	7.42	150
Kawamura	6.4	3.2	128	66	128	9.0	0.8–11.8	4.5	180
Kuroda	5π	2π	128	96	128	18.4	0.08–4.9	7.4	150

second-order Adams–Bashforth method was used for the explicit time integration of the convection terms, the viscous terms and the external-force terms. The fractional-step method was adopted for the implicit time integration of the pressure terms.

In the discretised form of Eq. (3), the reaction force to F_D for each bead was distributed to eight neighbouring grid points for forces by a spatial interpolation method. Similarly, the fluid velocity near a bead in the right-hand side of Eq. (1) was calculated from the values at eight neighbouring grid points for velocities by the spatial interpolation method.

3.4. Initial and boundary conditions

The result of a preliminary computation without the cluster models was adopted as the initial velocity field of the main computation after a statistically developed state was confirmed. The universal velocity distribution superimposed on sinusoidal velocity fluctuation in the three directions was taken as the initial velocity field for the preliminary computation. This velocity field satisfied the local and overall mass conservation.

200 cluster models were distributed nearly uniformly in the buffer region ($10 < X_2^+ < 30$) of the database at the initial state in the case where the region for each model was the cube. A total of 100 models whose initial region was rectangular prism were distributed nearly uniformly in two buffer regions ($10 < X_2^+ < 30$ and $270 < X_2^+ < 290$) to calculate turbulence quantities. These distributions are based on the experiment carried out by Tiederman et al. and our observation. The volume fraction and thus the concentration of the cluster models was estimated from the total number and the volume of the beads. The concentration was 20 ppm for all the computational domain and 450 ppm for the buffer region. This is comparable to 500 ppm for the case referred to in one of the experimental conditions by Miyamoto (see Table 1), and from 100 to 400 ppm in the case of our experiment and Tiederman's experiment.

The initial location of the beads was uniform in the initial cluster region mentioned above. The springs were arranged so that only the nearest two beads can be connected by one spring for the initial beads arrangement. This prevented unrealistic over-entanglement, such as the situation where beads diagonally positioned were also connected by the springs. All the beads have no slip velocity in the initial state.

The nonslip boundary condition was imposed for the walls. The periodical boundary condition was applied for velocity components, pressure and the cluster models in the X_1 and X_3 directions. Some of the cluster models lifted-up and transported in the core region stay in this region for a long time due to periodical boundary condition in the streamwise direction. This is not the same situation as in the experiment carried out by Tiederman et al. and present authors mentioned below. In order to avoid this discrepancy, the model was removed from the region and redefined in the buffer region, when a bead of any cluster model reached $X_2^+ = 150$.

4. Experimental observation for entangled PEO

We carried out an experiment for the simultaneous visualisation of the low-speed streaks and flowing highly entangled PEO in a turbulent duct flow to estimate the volume of the cluster model. Fig. 2 shows the experimental apparatus. The test section was the fully developed region in the horizontal duct of 2000 mm in length, $2h = 20$ mm in height and 160 mm in width. A dilute solution of PEO was injected into the main flow from a transverse slot 1.0 mm in streamwise width at 45° on the duct upper wall. The injection flow rate was adjusted so that the solution was introduced into the buffer region of the main flow. This method is similar to that used by Tiederman et al. The ratio of the flow rate per unit transverse length for the injection to that for the main flow was about 0.0065.

We adopted small pieces of an acrylic polymer-emulsion colour as tagging material for highly entangled PEO in the flow. These pieces were confirmed to stick to the polymer for a long time in the solution. An aqueous solution of Rhodamine B was injected into the linear sublayer from the other slot in

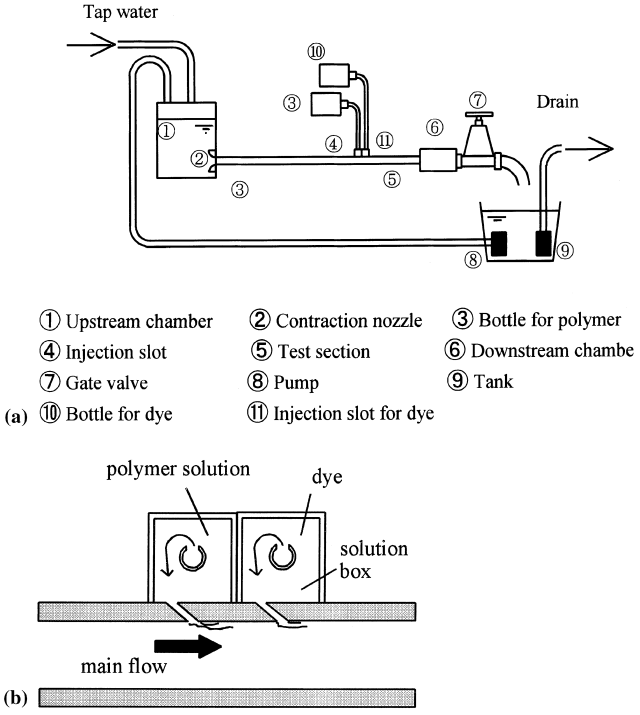

Fig. 2. Experimental apparatus: (a) schematic diagram; (b) injection slots.

order to visualise the low-speed streaks, which is similar to that carried out by Tiederman et al. (1985).

The images of the small pieces of the colour and the dye were captured by a progressive-scan video camera. The output signal of the video camera was directly recorded into a PC as digital images through a frame grabber. The Reynolds number based on the mean centerline velocity was 5.25×10^3.

5. Results and discussion

5.1. Estimation of the volume of entangled polymers

It was observed in the captured images that some groups of colour pieces (that is highly entangled polymers) were transported downstream. Fig. 3 is a typical frame captured. The white dots in the figure show colour pieces. The dimension of the group was in the range of $0.94 \sim 1.9$ mm. Assuming that the core region of the entangled polymers has a spheroidal shape, the volume of the region was determined. The range of the volume was shown in the nondimensional form in Table 1. Note that the increase in the transverse spacing of the low-speed streaks and the attenuation of the streamwise vortices were also observed with this apparatus in nearly identical flow conditions (Imamura et al., 1999; Hagiwara et al., 2000).

5.2. Turbulence quantities

The following statistical turbulence quantities were calculated from the ensemble averages over space and time for $1050\nu/u^{*2}$ from $t^+ = 450$. In the following figures, the open circles indicate the values in the case without the cluster models (i.e., the Newtonian fluid), and the solid circles indicate those in the case with the models. The DNS results of the spectral method by Kuroda et al. (1995) are also drawn.

Mean velocity and turbulence intensities: Fig. 4 shows the mean velocity profile. This velocity is slightly decreased in the buffer region and increased in the log region by the cluster models. This is in qualitative agreement with the experimental result,though the decreasing or increasing rate is less than the experimental data (Luchik and Tiederman, 1988). This discrepancy is consistent with the result and discussion by Toonden et al. (1999) that the increase in the mean velocity due to the polymer model was underestimated in case of DNS for much lower Reynolds number than their experiment.

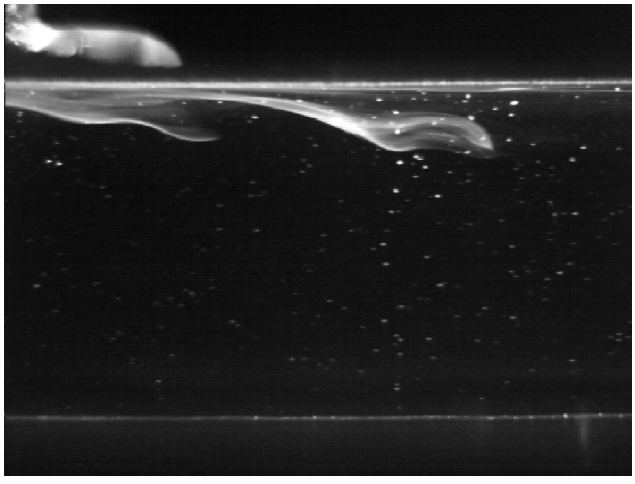

Fig. 3. Typical image of visualised PEO lumps (white dots) and low-speed streaks (white area).

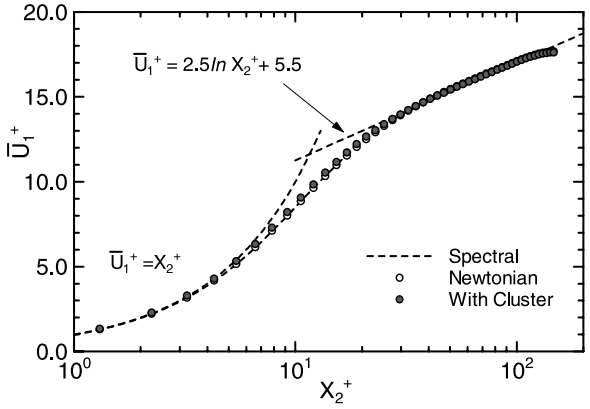

Fig. 4. Mean velocity profile.

It is found from Fig. 5 that the turbulence intensity in the streamwise direction is increased while those in the wall-normal and transverse directions are decreased in the buffer region by the cluster models. These results are also in qualitative agreement with the experimental results (Luchik and Tiederman, 1988).

Reynolds-shear stress: Fig. 6 demonstrates the profiles of the Reynolds-shear stress, $\overline{u_1 u_2}$, and the mean shear stress, $\mathrm{d}\overline{U}_1/\mathrm{d}X_2$. The Reynolds-shear stresses are found to be lower in the case with the cluster models than in the case without the models. This shows that the turbulence structure and its dynamics were attenuated by the cluster models. This attenuation causes the slight deficit of the total shear stress, $-\overline{u_1 u_2} + (1/Re)\mathrm{d}\overline{U}_1/\mathrm{d}X_2$. This is consistent with the experimental results for a slight decrease in the wall shear stress measured by Luchik and Tiederman (1988).

Turbulent kinetic energy: Fig. 7 indicates the budget of turbulent kinetic energy. The production and dissipation of the turbulent kinetic energy in the case with the cluster models are found to be slightly lower than in the case without the models. The attenuation of the production is due to the decrease in the Reynolds-shear stress by the models.

Fig. 8 demonstrates the orthogonal components of the pressure–strain terms, that is, the redistribution terms. The absolute values of all the terms are found to be decreased by the cluster models particularly in the buffer region. This shows that the redistribution of the turbulent kinetic energy in the streamwise direction to those in the other directions was attenuated. Therefore, it is expected that the vortical motion contributing to the redistribution mechanism of the turbulent

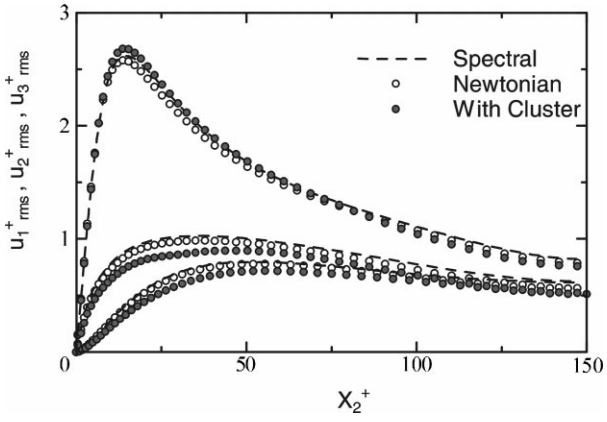

Fig. 5. Turbulence intensities.

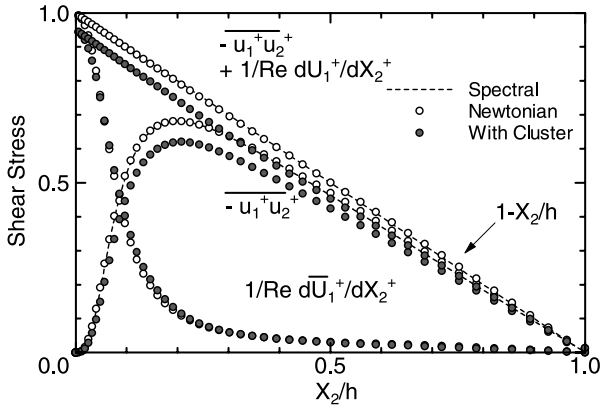

Fig. 6. Shear stress distribution.

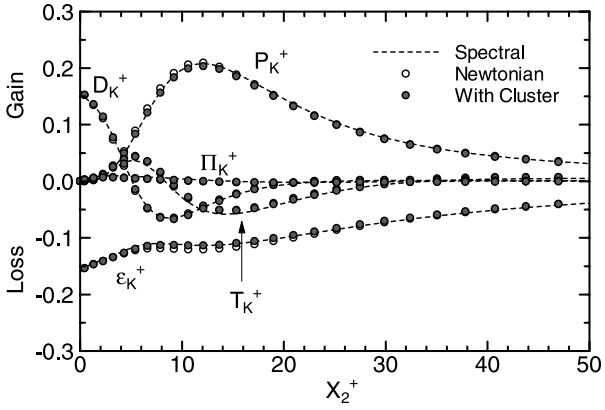

Fig. 7. Budget of turbulent kinetic energy.

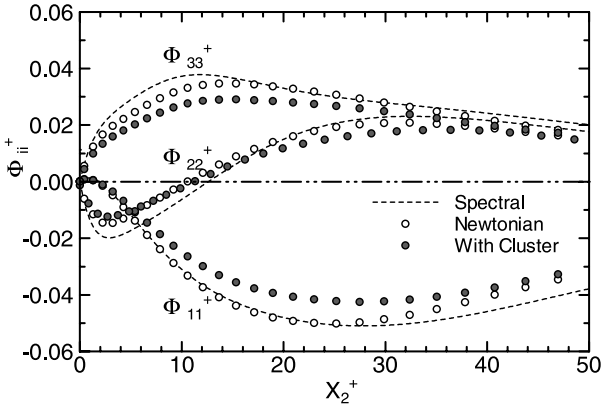

Fig. 8. Redistribution terms.

kinetic energy was attenuated by the cluster models. The modification of the redistribution terms is in agreement with the DNS result obtained by Kajishima and Miyake (1998).

5.3. Location of the cluster models, the streaks and the vortices

In the following, we focus on our result in the early stage before the beginning of the aforementioned ensemble average. This is because we can compare directly the result in the case with the cluster models with that in the case without the models, and discuss the direct effect of the models without considering the indirect effect of the accumulated interaction for a long time.

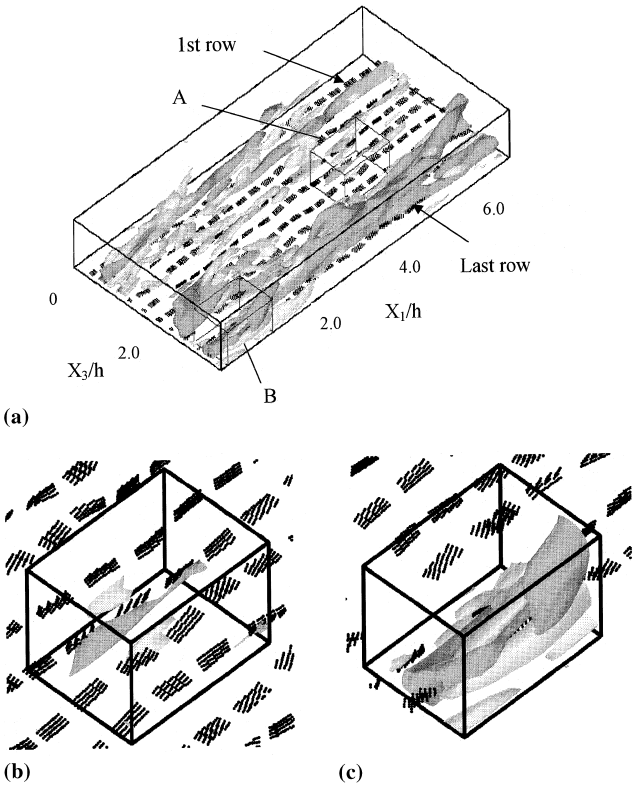

Fig. 9. Snapshot of cluster models, low-speed streaks and streamwise vortices ($t^+ = 6.0$) (rectangular prism cluster models): (a) bottom half of the computational domain; (b) magnified view of region A; (c) magnified view of region B.

Fig. 9(a) shows the snapshot of the cluster models in black, the low-speed streaks in dark grey and the streamwise vortices in light grey in the bottom half of the computational domain at $t^+ = 6.0$. Figs. 9(b) and (c) indicate the magnified part of the small boxes A and B in Fig. 9(a), respectively. We defined the low-speed streaks as the regions where $u_1 < -3.0u^*$ (u_1 is the fluctuating component of the streamwise velocity). The area in which the absolute values of the streamwise vorticity is larger than $0.2u^{*2}/\nu$ was regarded as the streamwise vortices based on the DNS study by Tsujimoto and Miyake (1998). This coherent structure is basically identical with that in the case without the cluster models at the same instant.

Three major low-speed streaks are seen in this figure. The largest streak is seen in the area of $2.5 < X_3/h < 3.0$. This streak was lifted up around $X_1/h > 4.0$, and the top of the streak reached midplane of the channel (the upper surface of the box in Fig. 9(a)). The diffusion associated with the ejection and the bursting are observed in this streak. Two other streaks are seen in the area of $0 < X_3/h < 0.8$. Two minor low-speed streaks are also seen in the central area. These minor streaks are found from the successive results to develop into major streaks as time proceeds. A pair of streamwise vortices is found to be adjacent to some part of all these streaks (see Figs. 9(b) and (c)). These vortices are counter-rotating as shown in Figs. 11 and 13. These vortices are confirmed to be associated with the dynamics of the streaks from the numerical results at an advanced time. The average streak spacing in the transverse direction was about 120 viscous wall units. Four or five streaks were observed through the period of ensemble average. These

Table 3
Comparison of scales

	Transverse length	Duration
Cluster model	14.7	$0.34 < t < 1.3$
Minor streaks	$\cong$ 15	–
Low-speed streaks	$\cong$ 40–70 [100]	$-[\cong 480]$
Ejection	$\cong$ 20[10–30]	$-[\cong 20]$
Eruption	$\cong$ 15	<4
Streamwise vortices	$\cong$ 40	–

results are similar to those of DNS conducted by other researchers (for example, Robinson et al., 1990).

Most cluster models in the first and second rows from the transverse boundary in the upper left of the domain are found to be inside or near two major streaks. A few cluster models in the fourth, fifth and seventh rows are near two minor streaks. The orientations of the cluster models close to both the minor streak and the minor (developing) streamwise vortex are found to be totally different from those of the other models, which were stretched in the streamwise direction by the mean shear (See Fig. 9(b)). This indicates that these models are affected by the local flow associated with the streak or the vortex. Many cluster models in the eighth, ninth and tenth rows are near or inside the largest streak. These models are affected by the local flow related to the streak. In particular, the models seen in Fig. 9(c) are highly deformed.

In Table 3, the transverse length and the characteristic time of the cluster are compared with the transverse length and the duration of the streaks in the present computation. The data with brackets in the table are based on the summary by Meng (1998). The lengths of the minor streaks and the eruption of the low-speed streaks mentioned below are found to be comparable to that of the cluster.

5.4. Reynolds-shear stress product

Attenuation and enhancement of product: Fig. 10 demonstrates the contour map of the difference between positive values of the Reynolds-shear stress product with clusters, $-u_1u_2$, and that without clusters in the plane $X_2^+ = 15$ at the same instant as that of Fig. 9. This is the direct comparison of Q2 or Q4 event for these two cases. Broken lines indicate negative values of the difference, thus decreases in the values of the product. The contour level is $-0.02, -0.04, -0.06$ and $-0.08u^{*2}$. Solid lines indicate increases in the values of the product. The contour level is 0.02, 0.04, 0.06 and $0.08u^{*2}$. The squares A and B in this figure correspond to the boxes A and B in Fig. 9(a), respectively.

Four different types of contours are seen in Fig. 10. First, the product is unchanged in some small areas. Almost all the cluster models in these areas are found to be irrelevant to the coherent structure.

Second, the contiguity of the positive contour and the negative contour is seen in some areas, such as $0 < X_3/h < 0.8$. Most cluster models in this area are partly inside the vortices or streaks. The velocity of the model centre was between that at one end of the model and that at the other end. The velocity difference, thus the drag force at one end of the model is opposite to that at the other end. This is the reason for the contiguity. As a result, net increase or decrease in the Reynolds-stress product due to these cluster models over the whole plane is not expected for the moment.

Third, the cluster models near the minor streak in Fig. 9(b) is found not to enhance but to attenuate the shear stress product. The shear stress product decreased more than $-0.04u^{*2}$ and the outward fluctuating velocity $+u_2$ attenuated

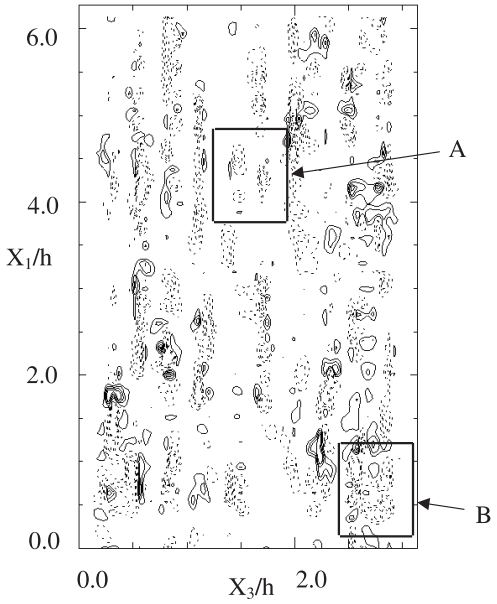

Fig. 10. Contour map of the difference between the Reynolds shear stress product with cluster models and that without cluster models (contour level = 0.02, 0.04, 0.06, $0.08u^{*2}$ for solid lines, = −0.02, −0.04, −0.06, $-0.08u^{*2}$ for broken lines).

more than 5%. These results suggest that the interaction between the cluster models and the minor streak may attenuate the Q2 event associated with the streak or its relevant vortex.

Finally, the cluster models inside the largest streak in Fig. 9(c) enhance the Reynolds-shear stress product in a narrow region and attenuate it in a wide region noticeably. The difference in the shear stress product reached more than $\pm 0.04u^{*2}$ in some narrow regions. This is not the same as the second type of change in the product. The last two types of interaction between the models and the turbulence structure are expected to contribute to the attenuation of Q2 event. Therefore, the velocity field is discussed below.

Streamwise dimension of contour: The contour map represents not only instantaneous interaction between the cluster model and the local turbulence structure but also 'footprint' or the evidence of the previous interactions. In order to understand this indirect effect, we compared the streamwise dimension, L_R, for the region in which the Reynolds-shear stress product is affected with the distance, L_T, for the cluster to be transported for the period through which the cluster gives the reaction of the drag force, $\boldsymbol{F}'_D$, on the grid point. L_T was about 0.4 h in this case. L_R associated with the cluster irrelevant to the streaks is shorter than L_T. On the other hand, L_R associated with the cluster near or inside the streaks is found to be longer than L_T even in the case of minor streaks. This shows that the modification of the fluctuating velocity around the distant cluster exerts an influence on the product through the velocity field even after the direct effect of the cluster vanishes. This is consistent with the aforementioned attenuation of the redistribution mechanism of turbulent kinetic energy in the streamwise direction to those in the other directions by the cluster models. The aforementioned effects of the cluster were also observed in the case where the initial region for each cluster was the rectangular prisms.

5.5. Minor streak–cluster interaction

Fig. 11 shows the instantaneous velocity field in the (X_2, X_3)-plane at $X_1 = 4.6\ h$ in the region A in Fig. 9(a), including

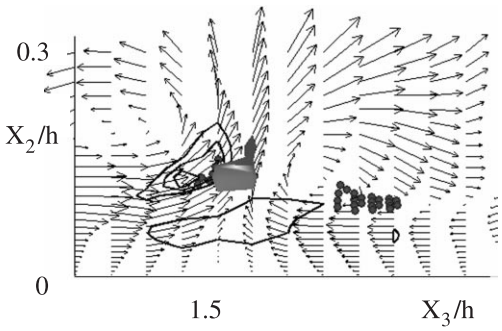

Fig. 11. Velocity field in the (X_2, X_3)-plane at $X_1 = 4.6\ h$ in the region A with the cross sections of the minor streak, the beads and the contours of the difference between the wall-normal velocity with cluster models and that without cluster models (contour level = 0.005, 0.010, $0.015u^*$).

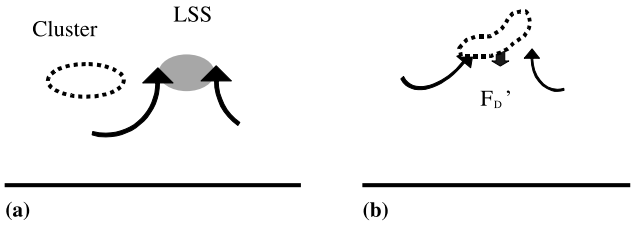

Fig. 12. Conceptual model for the attenuation of Q2 event near the minor streak: (a) while the cluster model approaches the streak: (b) while the model is deformed.

the cross sections of the minor streak drawn in Fig. 9(b) in black and the beads of the cluster model in solid circles. Note that the diameter of the beads is about three times larger than the actual diameter. The contours are also drawn in this figure for the difference between the wall-normal velocity with cluster models and that without cluster models. The flow from a left-hand side of the streak changed its direction from transverse to outward near the streak. The outer shape of the cluster model on the plane was deformed from horizontal oval to crescent by this change in the flow direction while it was transported from left to right in the figure. The springs in the model acted to recover the model shape. Thus, the relative motion is generated to the beads, then the drag force in the outward direction was generated on the beads. At the same time, $\boldsymbol{F}'_{\mathrm{D}}$ acted as a resistance to the outward flow (see Fig. 12). Thus, the outward fluctuating velocity decreased, and the Q2 event and the Reynolds-shear stress product were attenuated. Since the transverse length of the streak is comparable to the cluster dimension, this attenuation of the shear stress product occurred in the whole region of the streak. Therefore, the minor streak became inactive, and the evolution of the streak was prevented. This is expected to be one of the reasons for the decrease in the streaks observed by Tiederman et al. (1985).

5.6. Large-scale streak–cluster interaction

Fig. 13 shows the velocity field in the (X_2, X_3)-plane at $X_1 = 0.54\ h$ including the cross sections of the large-scale streak in black and the beads of the cluster in solid circles. The contours in this figure indicate the difference between the wall-normal velocity with cluster models and that without cluster models. As shown in Table 3, this streak has a larger transverse length and longer time scale compared with those of the cluster model.

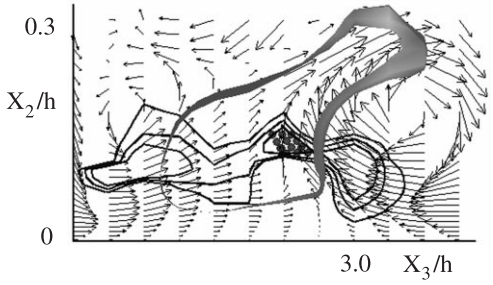

Fig. 13. Velocity field in the (X_2, X_3)-plane at $X_1 = 0.59\ h$ in the region B with the cross sections of the minor streak, the beads and the contours of the difference between the wall-normal velocity with cluster models and that without cluster models (contour level = 0.005, 0.010, $0.015u^*$).

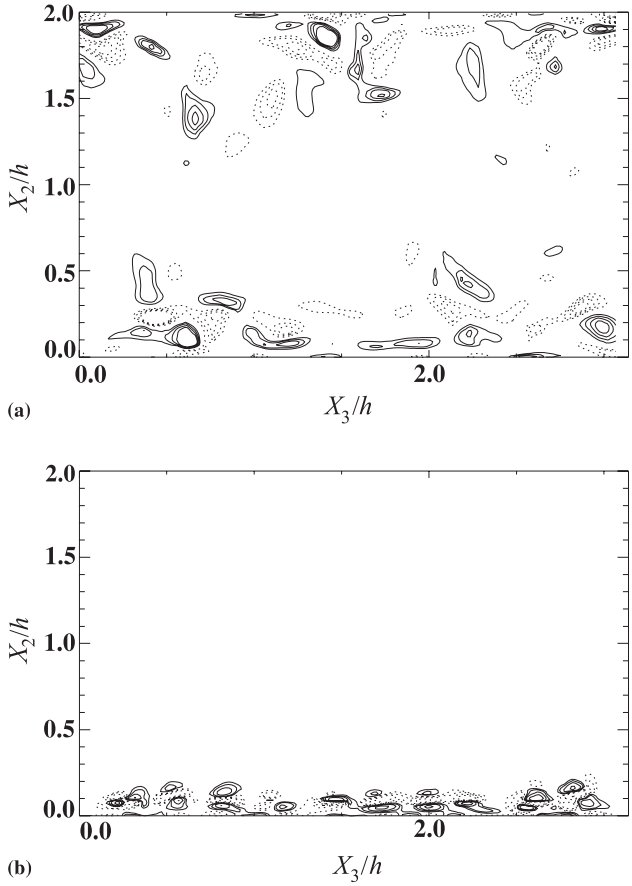

Fig. 14. Contour maps of the streamwise vorticity and its difference: (a) the streamwise vorticity (contour level = 0.10, 0.15, 0.20, $0.25u^{*2}/\nu$ for solid lines, $= -0.10, -0.15, -0.20, 0.25u^{*2}/\nu$ for broken lines); (b) the difference between the streamwise vorticity with cluster models and that without cluster models (contour level = 0.001, 0.002, 0.004, $0.008u^{*2}/\nu$ for solid lines, $= -0.001, -0.002, -0.004, 0.008u^{*2}/\nu$ for broken lines).

A strong outflow is observed to penetrate the thin streak. This flow was found to be characterised by the following events: u_2 increased with the distance from the wall in the buffer region, and a converged flow was induced by the outflow in the buffer region. The streamwise length of the outflow was

not so long compared with the transverse length of the flow (about $15\nu/u^*$). The duration was estimated to be shorter than $4\nu/u^{*2}$. From observations, this flow appears to be similar to the eruption of the low-speed streaks studied by Smith and Walker (1995) and Zhou et al. (1999). The eruption is considered to be self-sustenance of the quasi-streamwise vortices and to be followed by a bursting event.

Part of the outflow is found to approach the cluster model. The strong drag force is generated on the beads by the nonuniform distribution of u_2 in the eruptive flow. At the same time, $\boldsymbol{F}'_{\mathrm{D}}$ attenuates the outflows noticeably. Also, the wall-normal velocity of the fluid coming into the eruptive part is found from the contours to be attenuated in a wide region. These lead to an attenuation of the eruptive flow.

This effect of this cluster model on this eruptive flow resulted in the attenuation of self-sustenance of the quasi-streamwise vortex appearing in the right-hand side of the cluster in Fig. 13. Fig. 14(a) demonstrates the contour map of the streamwise vorticity, ω_1, in the case with cluster models and Fig. 14(b) shows the difference between the vorticity with clusters and that without clusters in the plane $X_1^+ = 0.54$ at $t^+ = 6$. Broken lines indicate negative values and thus the vorticity decreases in the region drawn by the lines. It is found that the streamwise vorticity for the quasi-streamwise vortex in the right bottom of the figure was attenuated by the cluster model in Fig. 13. This is due to the attenuation of the eruptive flow, effective for the sustaining mechanism of the vortex, by the cluster model. This result is consistent with that simulated by Orlandi (1995). This could be a reason for the decrease in the bursting rate measured by Tiederman et al. (1985).

6. Conclusions

Direct numerical simulation was carried out for a turbulent channel flow with many cluster models of beads and springs representing highly entangled polymers in the buffer region. The main conclusions are as follows:

1. The dimensions, number density and apparent spring constant of the present cluster model are comparable to those of real entangled polymers.
2. The minor streaks, which may develop into large-scale streaks, was attenuated by the cluster model whose transverse length and duration are comparable to those of the minor streaks.
3. The cluster model attenuates the strong eruptive outward flows, whose transverse length scale and relaxation time are comparable to those of the cluster, associated with the large-scale low-speed streaks.
4. These effects of the cluster model on the small-scale near-wall coherent structure can be regarded as the cause of the observation made by Tiederman et al. (1985).

Acknowledgements

The authors acknowledge Mr. T. Imamura, the graduate student at Kyoto Institute of Technology, for his assistance. This work is partially supported by the Ministry of Education, Science, Culture and Sports through the Grant-in-Aid for Scientific Research (No. 11650222).

Appendix A

In the second-order central difference scheme with the interpolation method, the gradient form of the convection term was evaluated not at the grid point but at half the grid-spacing in the direction of convection from the grid point. Then the interpolated value of two adjacent gradient forms in the direction of convection was assigned at the grid point between the two points where the forms were evaluated. This evaluation satisfies numerical consistency between the mass continuity and the momentum convection in case of uniform grid arrangement. Kawamura reported that the computational results of low-order turbulence quantities and the time change and the budget of turbulent kinetic energy using this scheme showed good agreement with the results obtained using the spectral method even in the case for nonuniform grid arrangement shown in Table 2.

The convection terms for the velocity of U_1 are expressed as follows:

$$
\begin{aligned}
&U_1 \frac{\partial U_1}{\partial X_1}\bigg|_{i+1/2,j,k} + U_2 \frac{\partial U_1}{\partial X_2}\bigg|_{i+1/2,j,k} + U_3 \frac{\partial U_1}{\partial X_3}\bigg|_{i+1/2,j,k} \\
&\quad = \frac{1}{2}\Bigg[\Bigg(\frac{U_1|_{i+3/2,j,k} + U_1|_{i+1/2,j,k}}{2} \cdot \frac{U_1|_{i+3/2,j,k} - U_1|_{i+1/2,j,k}}{\Delta X_1} \\
&\qquad + \frac{U_1|_{i+1/2,j,k} + U_2|_{i-1/2,j,k}}{2} \cdot \frac{U_1|_{i+1/2,j,k} - U_1|_{i-1/2,j,k}}{\Delta X_1}\Bigg) \\
&\qquad + \Bigg(\frac{U_2|_{i+1,j+1/2,k} + U_2|_{i,j+1/2,k}}{2} \cdot \frac{U_1|_{i+1/2,j+1,k} - U_1|_{i+1/2,j,k}}{(\Delta X_2|_{j+1} + \Delta X_2|_j)/2} \\
&\qquad + \frac{U_2|_{i+1,j-1/2,k} + U_2|_{i,j-1/2,k}}{2} \cdot \frac{U_1|_{i+1/2,j,k} - U_1|_{i+1/2,j-1,k}}{(\Delta X_2|_j + \Delta X_2|_{j-1})/2}\Bigg) \\
&\qquad + \Bigg(\frac{U_3|_{i+1,j,k+1/2} + U_3|_{i,j,k+1/2}}{2} \cdot \frac{U_1|_{i+1/2,j,k+1} - U_1|_{i+1/2,j,k}}{\Delta X_3} \\
&\qquad + \frac{U_3|_{i+1,j,k-1/2} + U_3|_{i,j,k-1/2}}{2} \cdot \frac{U_1|_{i+1/2,j,k} - U_1|_{i+1/2,j,k-1}}{\Delta X_3}\Bigg)\Bigg],
\end{aligned}
$$

where U_2 and U_3 are the velocity components in the X_2 and X_3 directions, respectively. The subscripts i, j and k denote the grid location in the X_1, X_2 and X_3 directions, respectively.

References

Gampert, B., Yong, C.K., 1990. The influence of polymer additives on the coherent structure of turbulent channel flow. In: Gyr, A. (Ed.), Proceedings of the IUTAM Symposium on Structure of Turbulence and Drag Reduction. Springer, Berlin, pp. 223–232.

Hagiwara, Y., Takashina, Y., Tanaka, M., Hana, H., 1997. A numerical simulation on the interaction between tangled polymers and turbulent structures. In: Proceedings of the 11th Turbulent Shear Flows, vol. 3, 28-19–28-24.

Hagiwara, Y., Hana, H., Murai, S., Tanaka, M., Maxey, M.R., 1998. Local effect of polymers used for drag reduction on turbulent solvent duct flow. In: Proceedings of the Third International Conference on Multiphase Flow, pp. 1–8 (CD–Rom).

Hagiwara, Y., Imamura, T., Takagaki, S., Tanaka, M., 2000. Direct interaction between highly-entangled polymers and small-scale coherent structures in a turbulent polymer-solution flow. In: Proceedings of the Eighth European Turbulence Conference (to appear).

Harder, K.J., Tiederman, W.G., 1991. Drag reduction and turbulent structure in two-dimensional channel flows. Philos. Trans. R. Soc. Lond. A 336, 19–34.

Imamura, T., Murai, S., Hana, H., Hagiwara, Y., Tanaka, M., 1999. The visualization of polymer clusters and low-speed streaks in a duct flow. In: Proceedings of the 36th National Heat Transfer Symposium of Japan, vol. 3, pp. 547–548 [in Japanese].

James, D.F., Saringer, J.H., 1980. Extensional flow of dilute polymer solutions. J. Fluid Mech. 97, 655–671.

Kajishima, T., 1994. Conservation properties of finite difference method for convection. Trans. JSME (B) 60, 2058–2063 in Japanese.

Kajishima, T., Miyake, Y., 1998. Drag reduction by polymer additives in turbulent channel flow simulated by discrete-element models. Trans. JSME (B) 64, 3636–3643 [in Japanese].

Kawamura, H., 1995. Direct numerical simulation of turbulence by finite difference scheme. In: The Recent Developments in Turbulence Research. Academic Publishers, New York, pp. 54–60.

Kuroda, S., Kasagi, N., Hirata, M., 1995. Direct numerical simulation of turbulent plane Couette–Poiseuille flows. In: Durst, F., et al. (Eds.), Turbulent Shear Flows 9, Springer, Berlin, pp. 241–257.

Luchik, T.S., Tiederman, W.G., 1988. Turbulent structure in low-concentration drag-reducing channel flows. J. Fluid Mech. 190, 241–263.

Massah, H., Kontomaris, K., Schowalter, W.R., Hanratty, T.J., 1993. The configurations of a FENE bead–spring chain in transient rheological flows and in a turbulent flow. Phys. Fluids A 5, 881–890.

Massah, H., Hanratty, T.J., 1997. Added stresses because of the presence of FENE-P bead–spring chains in a random velocity field. J. Fluid Mech. 337, 61–101.

Meng, J.C.S., 1998. Wall layer microturbulence phenomenological model and a semi-Markov probability predictive model for active control of turbulent boundary layers. In: Panton, R.L. (Ed.), Self-sustaining Mechanisms of Wall Turbulence. Comp. Mech. Pub., Southampton, pp. 201–252.

Miyamoto, H., 1994. Experiment for visualization of polymer chains in high-polymer aqueous solutions under shear flow regions. Trans. JSME (B) 60, 2038–2043 [in Japanese].

Oldaker, D.K., Tiederman, W.G., 1977. Spatial structure of the viscous sublayer in drag-reducing channel flows. Phys. Fluids 20, S133–S144.

Orlandi, P., 1995. A tentative approach to the direct simulation of drag reduction by polymers. J. Non-Newtonian Fluid Mech. 60, 277–301.

Pan, Y., Banerjee, S., 1996. Numerical simulation of particle interactions with wall turbulence. Phys. Fluids 8, 2733–2755.

Robinson, S.K., Kline, S.J., Spalart, P.R., 1990. Quasi-coherent structures in the turbulent boundary layer: Part II. Verification and new information from a numerically simulated flat-plate layer. In: Kline, S.J., Afgan, N.H. (Eds.), Near-Wall Turbulence. Hemisphere, Washington, DC, pp. 218–247.

Smith, C.R., Walker, J.D.A., 1995. Turbulent wall-layer vortices. In: Green, S.I. (Ed.), Fluid Vortices. Kluwer, Dordrecht, pp. 235–290.

Sureshkumar, R., Beris, A.N., Handler, R.A., 1997. Direct numerical simulation of the turbulent channel flow of a polymer solution. Phys. Fluids 9, 743–755.

Tiederman, W.G., Luchik, T.S., Bogard, D.G., 1985. Wall-layer structure and drag reduction. J. Fluid Mech. 156, 419–437.

den Toonder, J.M.J., Hulsen, M.A., Kuiken, G.D.C., Nieuwstadt, F.T.M., 1997. Drag reduction by polymer additives in a turbulent pipe flow: numerical and laboratory experiments. J. Fluid Mech. 337, 193–231.

Tsujimoto, K., Miyake, Y., 1998. Identification of quasi-streamwise vortices in near-wall turbulence and analysis of self-sustenance mechanism of them. Trans. JSME (B) 64, 1989–1996 in Japanese.

Warholic, M.D., Massah, H., Hanratty, T.J., 1999. Influence of drag-reducing polymers on turbulence: effects of Reynolds number, concentration and mixing. Experiments in Fluids 27 (5), 461–472.

Willmarth, W.W., Wei, T., Lee, C.O., 1987. Laser anemometer measurements of Reynolds stress in a turbulent channel flow with drag reducing polymer additives. Phys. Fluids 30, 933–935.

Zhou, J., Adrian, R.J., Balachandar, S., Kendall, T.M., 1999. Mechanism for generating coherent packets of hairpin vortices in channel flow. J. Fluid Mech. 387, 353–396.